Electronic Supplementary Material (ESI) for Journal of Materials Chemistry A.

Supporting Information

Chemical and photoelectrochemical instability of amorphous TiO2 layers quantified by spectroscopic ellipsometry

H. Kriegel,[a] J. Kollmann,[a] R. Raudsepp,[a] T. Klassen[ab] and M. Schieda*[a]

[a] Helmholtz-Zentrum Geesthacht, Centre for Materials and Coastal Research GmbH, Max-Planck-Str. 1, D-21502 Geesthacht, Germany. E-mail: mauricio.schieda@hzg.de

[b] University of the Federal Armed Forces, Helmut-Schmidt-University, Holstenhofweg 85, D-22043 Hamburg, Germany.

Spectrum of the used Xenon lamp

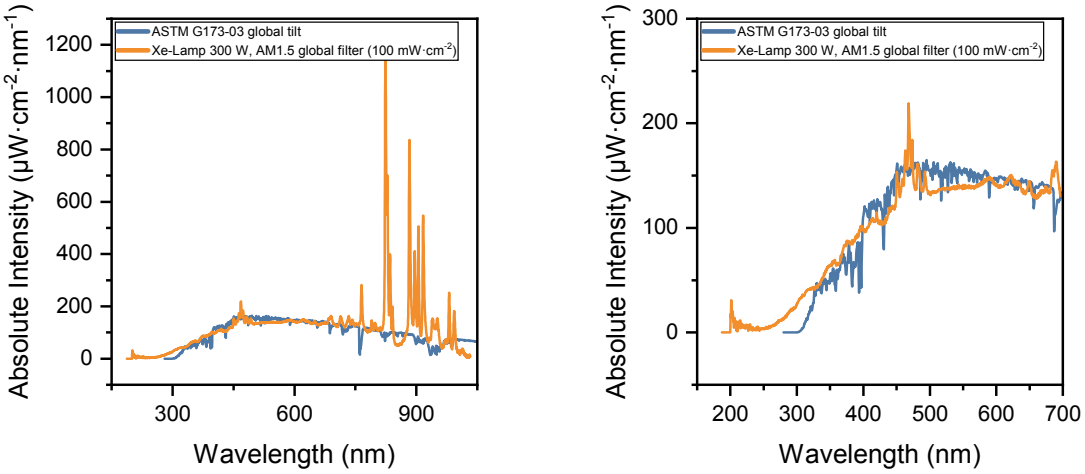

Fig. S1 Spectrum of the used 300 W Xenon lamp fitted with an AM1.5 global filter and reference solar spectral irradiance ASTM G173-03 global tilt shown in the range of 150-1050 nm and 150-700 nm.

Atomic Force Microscopy

Homogeneity investigation

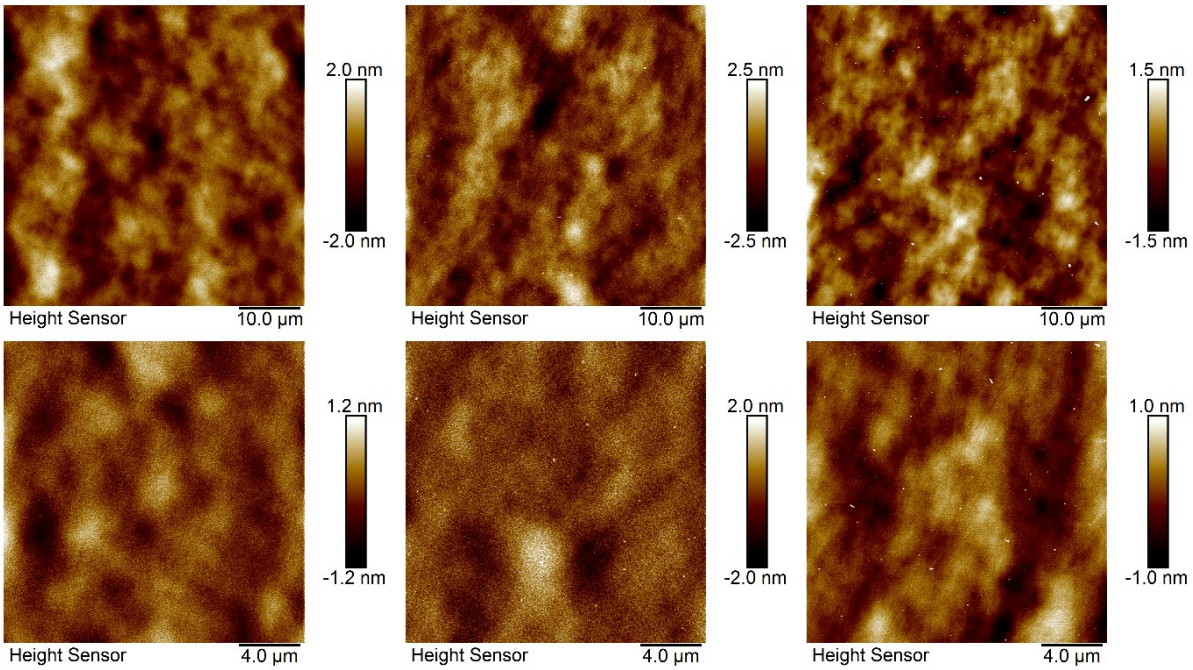

Fig. S2 AFM topography (Bruker Dimension Icon) of the amorphous ALD-grown TiO_2 coatings using quantitative nanomechanical (QNM) mapping AFM mode with PEAKFORCE-HIRS-SSB probes (1 nm radius) and DAFMCH-HA cantilever holder (Bruker). Amorphous TiO_2 films were exposed to 0.5 M H_2SO_4 under illumination with 100 mW/cm^2. (a) Before etching, (b) etched down to 28 nm TiO_2 thickness, (c) etched to complete removal of TiO_2 film. Peak force setpoint: 200-750 pN, scan rate: 0.2-0.3 Hz, tip velocity: 20-30 µm/s (for 50 µm scan size) and 8-12 µm/s (for 20 µm scan size), tip spring constant: 0.12 N/m.

As evidenced by the AFM micrographs, the degradation of ALD-grown amorphous TiO_2 films occurs homogenously at the nanometer scale. No anisotropy is observable in the height maps beyond the surface roughness of the samples. No holes or cracks can be observed on the TiO_2 film. Note the presence of particulate residue on the samples that were etched in electrolyte.

Evolution of roughness

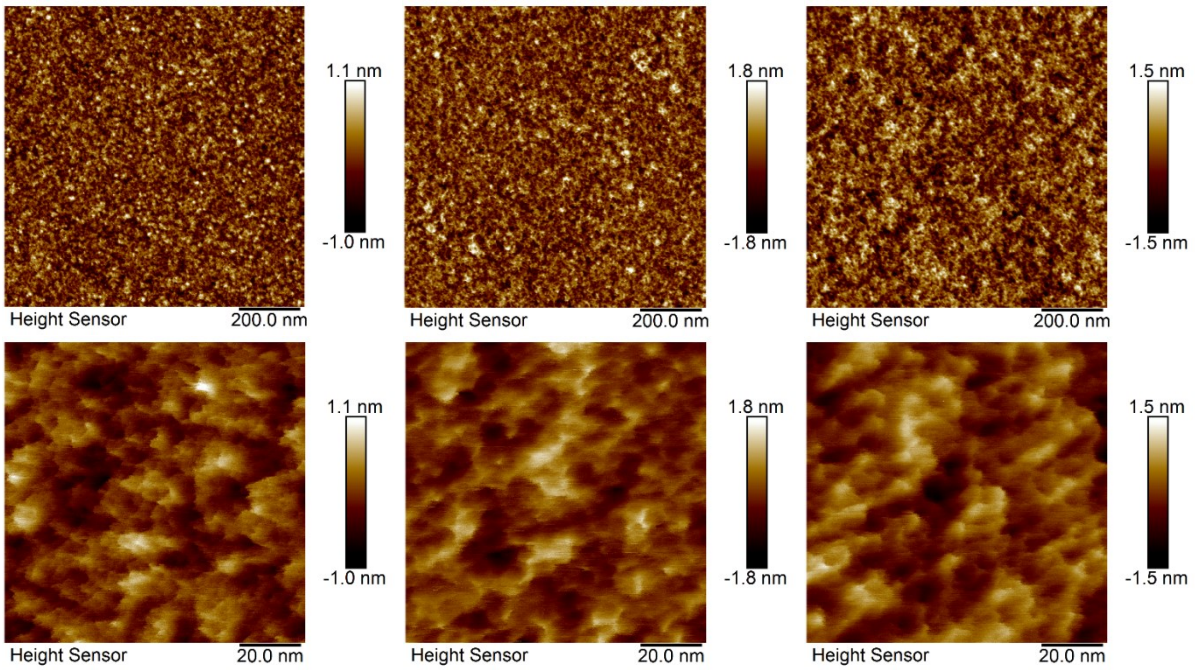

Fig. S3 AFM topography of the amorphous TiO_2 coatings using QNM mode measured on the ALD-grown, amorphous TiO_2 films (in the center of the electrolyte-exposed area) after exposing to 0.5 M H_2SO_4 at open-circuit potential under illumination with 100 mW/cm^2. (a) Before exposure, (b) 4 h exposure time, (c) 31.5 h exposure time. Peak force setpoint: 300 pN, scan rate: 0.3 Hz, tip velocity: 0.6 µm/s (for 1 µm scan size) and 3.0 µm/s (for 0.1 µm scan size), tip spring constant: 0.12 N/m.

Table S1 Arithmetic roughness (Ra) and root mean square roughness (Rq)(*) for untreated and exposed TiO_2 samples

	1 µm scan size		**0.1 µm scan size**	
Treatment time (h)	Ra (nm)	Rq (nm)	Ra (nm)	Rq (nm)
0	0.230	0.291	0.202	0.254
4	0.384	0.487	0.316	0.402
31.5	0. 361	0.452	0.295	0.366

(*) Arithmetic average roughness (Ra) is the arithmetic mean deviation of the absolute surface height values, whereas root mean square (RMS) average roughness (Rq) is the square root of the surface height distribution. They are expressed as:

$$Ra = \frac{1}{n}\sum_{i=1}^{n}|y_i| \qquad Rq = \sqrt{\frac{1}{n}\sum_{i=1}^{n}y_i^2}$$

Spectroscopic Ellipsometry

Model	Expression
Cauchy	$n(\lambda) = A + \frac{B}{\lambda^2} + \frac{C}{\lambda^4}$
Tauc-Lorentz	$\varepsilon_2 = \left[\frac{Amp \cdot E_0 \cdot Br \cdot (E - E_g)^2}{(E^2 - {E_0}^2)^2} \cdot \frac{1}{E}\right] for\ E > E_g$
Cody-Lorentz	$\varepsilon_2 = \begin{cases} \frac{E}{E_1} exp\left(\frac{(E - E_g - E_t)}{E_u}\right) & ;just\ above\ the\ bandgap\ (E < (E_g + E_t)) \\ \frac{(E - E_g)^2}{(E - E_g)^2 + E_p^2} \cdot \frac{Amp \cdot E_0 \cdot Br \cdot E}{\left[(E^2 - {E_0}^2)^2 + Br^2 E^2\right]} & ;at\ higher\ energies\ (E > (E_g + E_t)) \end{cases}$
Gaussian	$\varepsilon_{Gauss} = Amp\left\{\left[\Gamma\left(\frac{E - En}{\sigma}\right) + \Gamma\left(\frac{E + En}{\sigma}\right)\right] + i \cdot \left(exp\left[-\left(\frac{E - En}{\sigma}\right)^2\right] - exp\left[-\left(\frac{E + En}{\sigma}\right)^2\right]\right)\right\}$

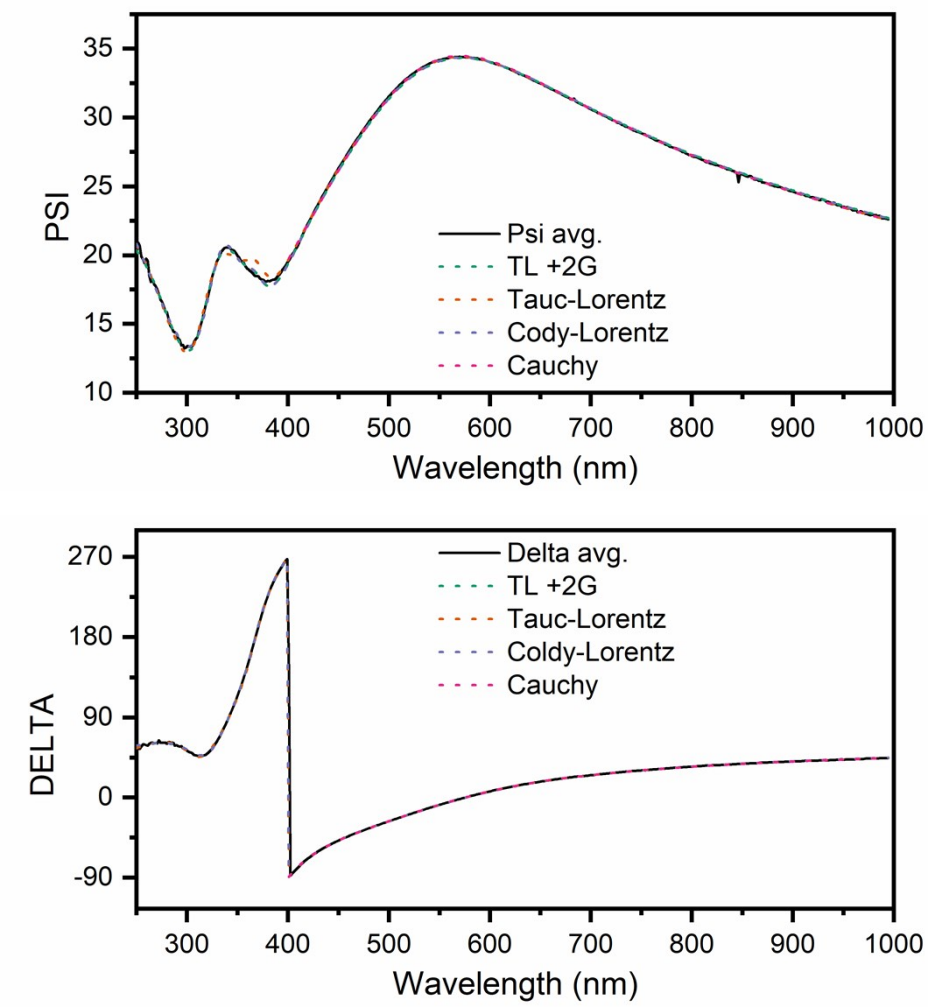

Fig. S4 Absolute values of PSI and DELTA for non-etched TiO_2 films measured and modelled with four dispersions (TL +2G represents a Tauc-Lorentz dispersion with two additional Gaussian oscillators).

As seen in Fig. S4, the various dispersions can be fitted very closely to the experimental data auf psi and delta. The Cauchy model is only applicable for transparent layers and was adapted only for wavelength >400 nm. A model with a single Tauc-Lorentz dispersion fits very closely over the entire range with the exception around 380 nm in the psi plot with a visible divergence. Using either 1-2 additional Gaussian oscillators in conjunction with Tauc-Lorentz or the Cody-Lorentz dispersion that accounts for sub-band gap absorption, no apparent mismatch between experimental and modelled data remains. Only miniscule differences remain as can be seen from the difference plots (Fig. S5).

The optical properties (Fig. S6) of the TiO_2 layer based on the different dispersions are similar over a wide range of wavelengths and result in very similar results for modelled film thickness but the value of the calculated band gap is systematically lower for the Tauc-Lorentz dispersion when compared to Cody-Lorentz or with added sub-band gap oscillators ("+2G").

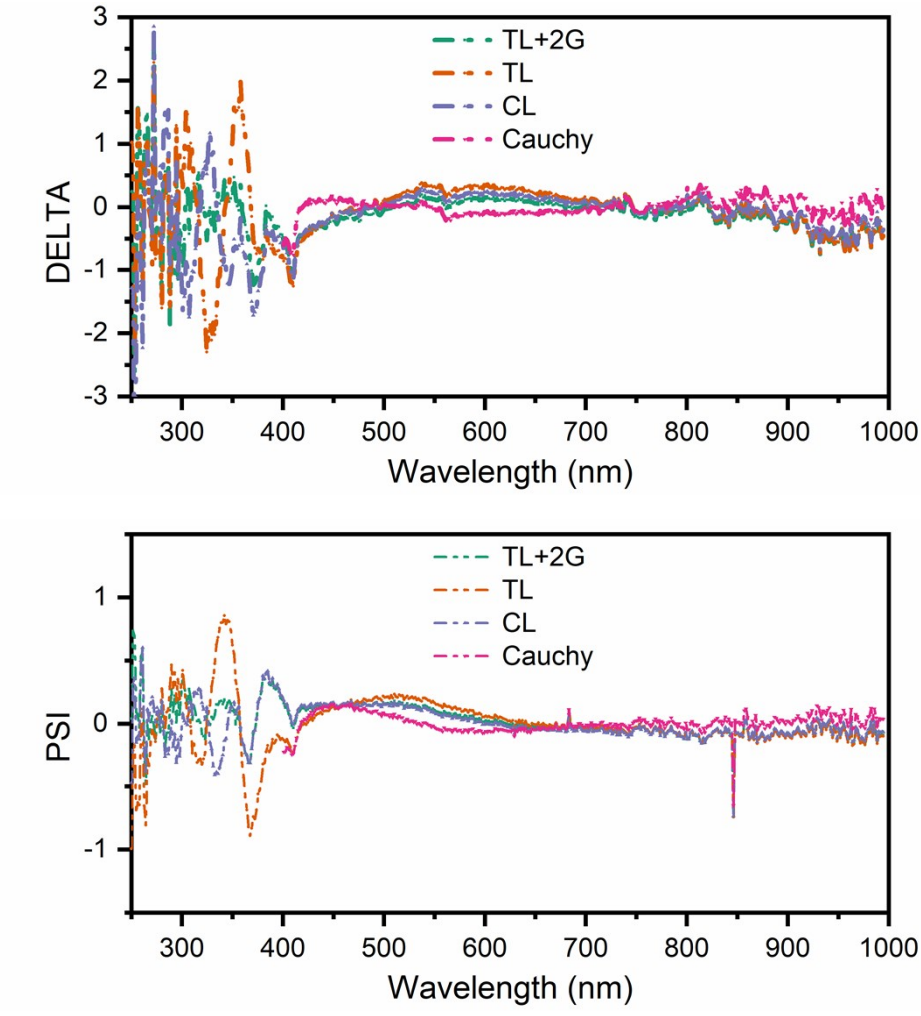

Fig. S5 Absolute difference of modelled and measured values for the four model dispersions of data above.

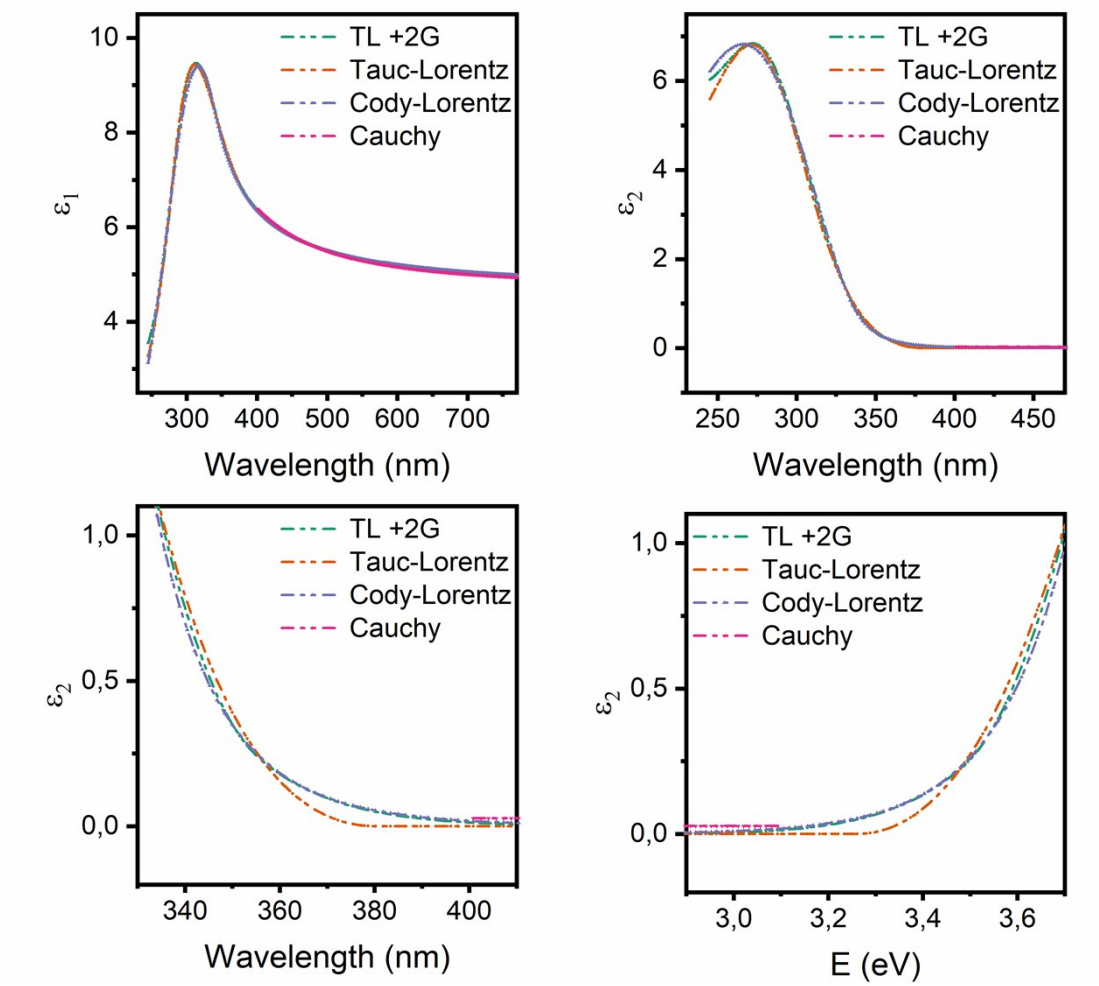

Fig. S6 Resulting real (ε_1) and imaginary (ε_2) part of the dielectric function for the TiO_2 layer, based on the four model dispersions.

Homogeneity investigation

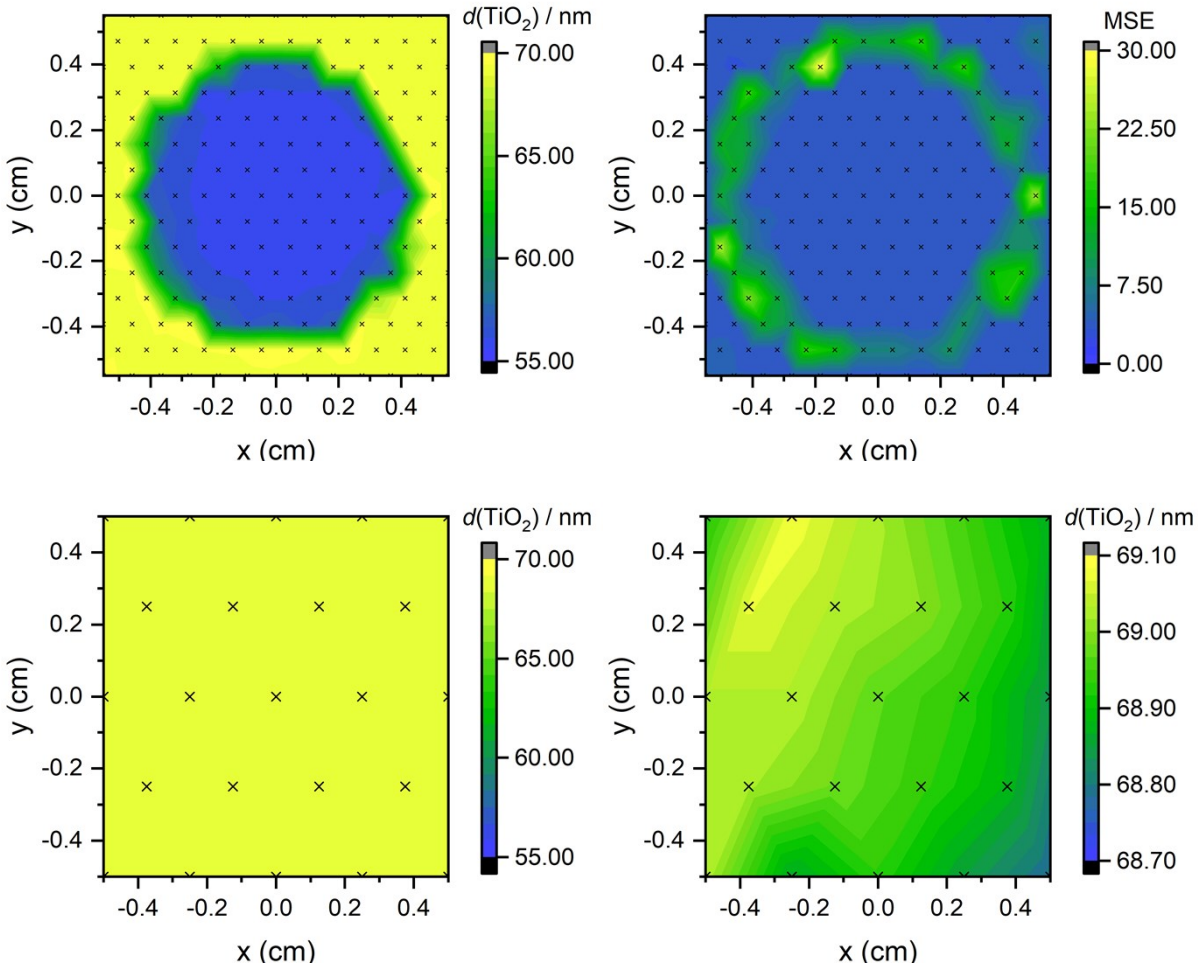

Fig. S7 Film thickness map (**top left**), obtained by fitting spectroscopic ellipsometry data, and mean squared error (MSE) of the fit (**top right**), for an etched, ALD-grown, amorphous TiO_2 film.

Notice that, for the etched sample, an o-ring had ensured sealing of the sample against the electrolyte compartment. The hexagonal grid of measurement points does not fully resolve the circular shape of the mark left by the o-ring. Furthermore, moving radially across the circular mark, the thickness changes from etched (inside the ring, in contact with the electrolyte) to unetched (outside the ring). The result is a higher MSE for the thickness fit in the annular area where the o-ring was touching the sample.

Bottom: film thickness map obtained for an unexposed TiO_2 film, plotted at two different height scales for reference.

All maps were measured at incidence angles of 60°, 65° and 70°, at each coordinate marked by a cross, using focusing probes with a spot size of a few hundred micrometers. The ellipsometry data were fitted using a Cauchy dispersion model in the transparent region of 400-2500 nm, with fixed Urbach absorption parameters for TiO_2.

Influence of dynamic thermal equilibrium: temperature profile

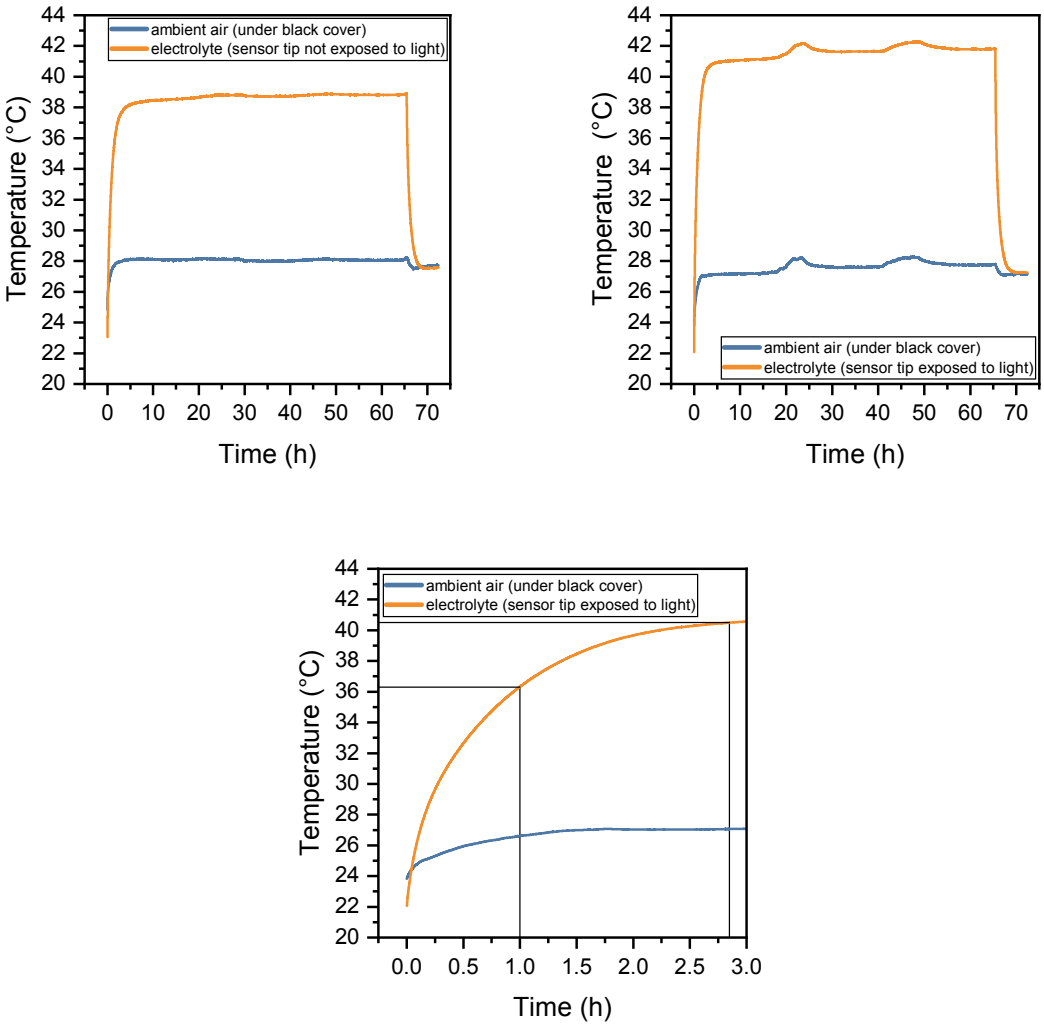

Fig. S8 Temperature profiles of the Pt-100 resistance thermometer with the sensor tip not exposed to light and with the sensor tip illuminated as well as the corresponding reference temperature profiles for the ambient air. The brief rises in temperature at 20 h and 40 h are due to an increased laboratory ambient temperature during the day.

Influence of dynamic thermal equilibrium: thickness profile

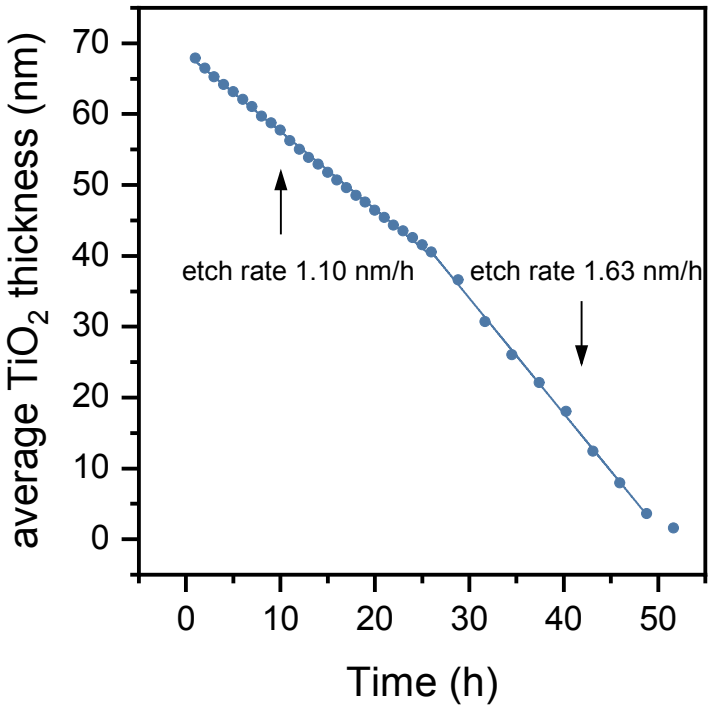

Fig. S9 Thickness profile of the amorphous TiO_2 layer under 100 mW/cm^2 illumination at open-circuit conditions in 0.5 M H_2SO_4. The average thickness of 49 points on the sample was measured *ex-situ* by spectroscopic ellipsometry after illumination of 1 h or 2.85 h.

According to Fig. S8 the illuminated sample reaches a temperature of 36.3 °C after 1 h and 40.5 °C after 2.85 h leading to etch rates of 1.10 nm/h and 1.63 nm/h respectively.

X-ray photoelectron spectroscopy

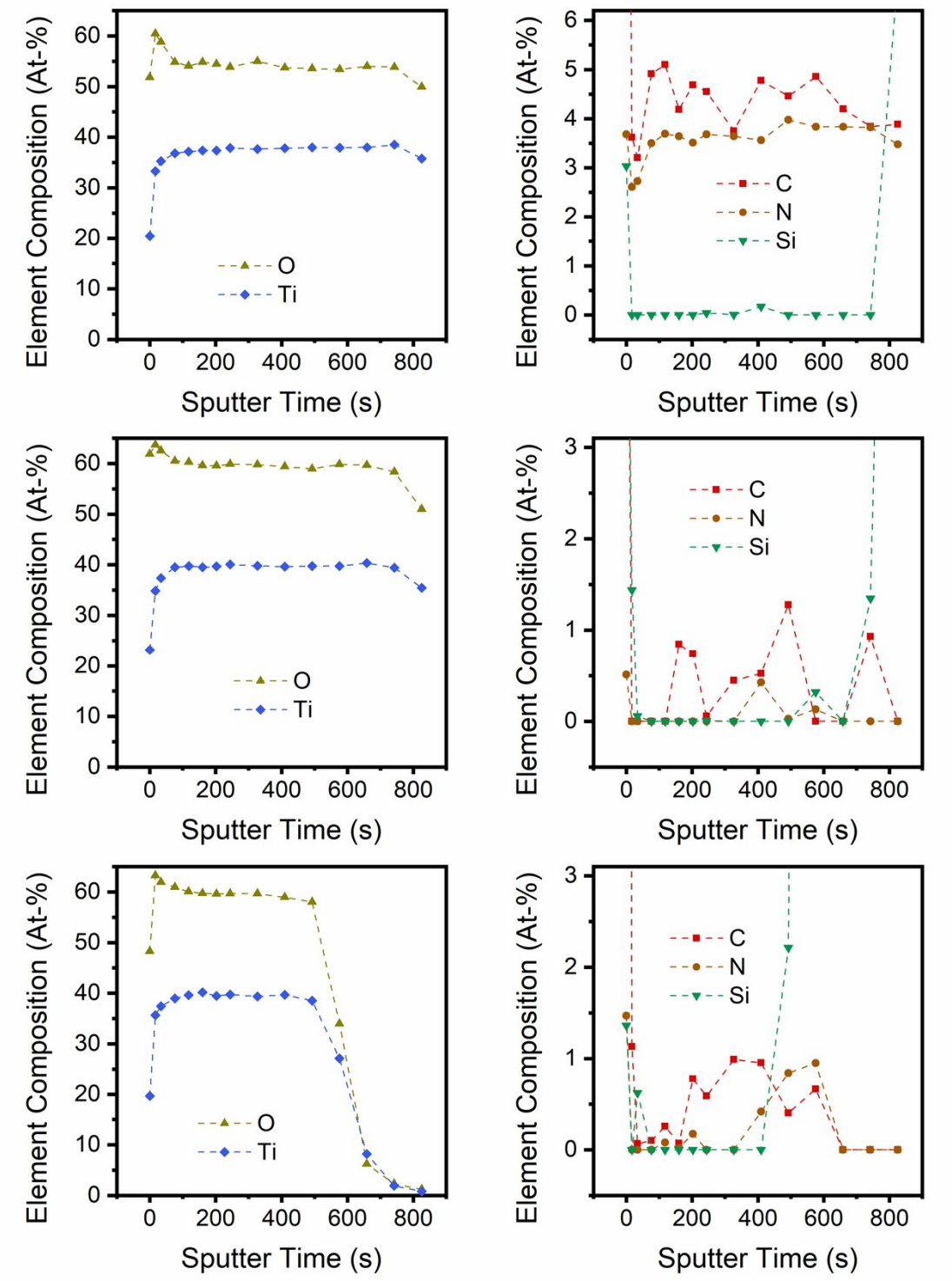

Fig. S10 XPS profiles of main constituents and impurities of TiO_2 films.

Top to bottom: Amorphous 100 °C deposition, crystalline 300 °C deposition, partially crystalline (thinner) deposition at 300 °C. Thermo VG Scientific K-Alpha, Al-Kα, ~75 W, 400 µm spot size, acquisition at 30 eV. Ar sputter with MAGICS-Ion source. The actual sputtering rate is material dependent, and thus slightly different for the three coatings. The appearance of the Si signals indicates that the interface to the substrate has been reached.

Electrochemical Impedance Spectroscopy

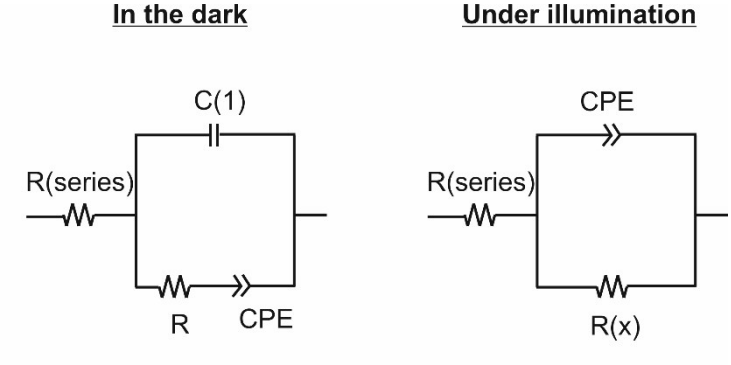

Fig. S11a-b Electrochemical equivalent circuits (EEC) used to fit results from impedance spectroscopy in for a blocking layer in the dark and conductive mechanism under illumination

The fitting and analysis of the electrochemical impedance spectroscopy over a potential from -0.1 V vs SHE to 1.7 V vs SHE with the equivalent circuits shown in the main text and Fig. S11, revealed several features that can be linked to the cyclic voltammograms in Fig. 5 of the main text.

Additionally to the capacitive peak at 0.25 V in the dark and resistance maximum under illumination at the same potential (Fig 6b-c, main text), the resistance element in dark conditions (Fig. S12b) shows the transition from a blocking layer (>0.3 V) to conduction at more cathodic potential with a sharp decrease in resistance in accordance to an onset of reduction current. Similarly, the capacitance derived from the constant phase element (CPE) changes drastically. Neither of the capacitances reflects Mott-Schottky-like behaviour for a semiconductor

Under illumination, the capacitance in the CPE vaguely resembles a linear trend for $1/C^2$ vs applied potential (Fig. S13a), descriptive for Mott-Schottky behaviour, which agrees with the generation of photocurrent even for amorphous TiO_2. The resistance is approximately constant at potential >0.8 V, rises to a peak at 0.25 V as described and decreases for more cathodic potential with the addition of dark reductive currents (Fig. S13b).

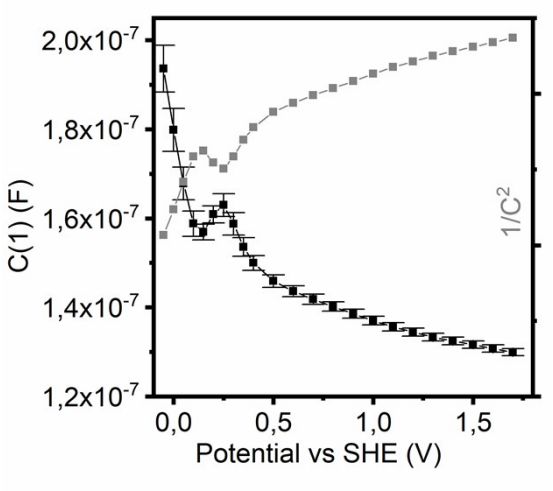

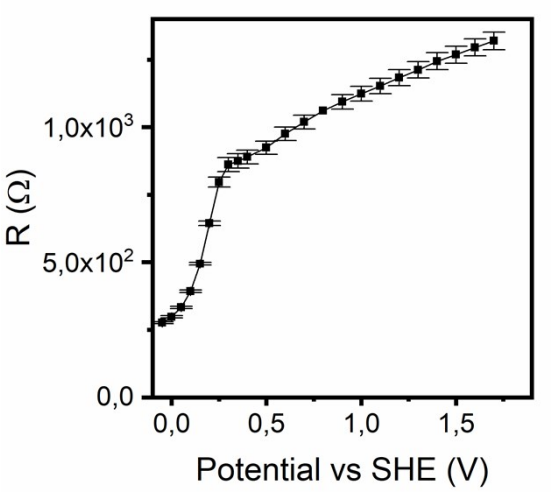

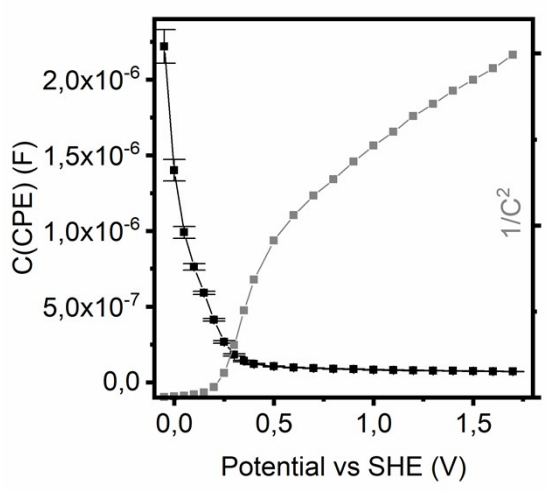

Fig. S12a-c Fitting data for EIS measurements in the dark with EEC Fig S11a.

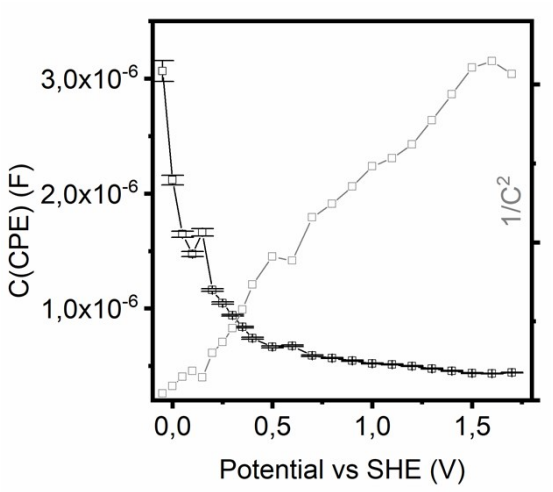

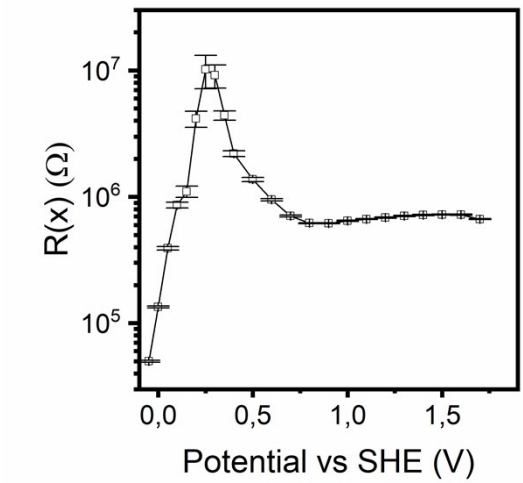

Fig. S13a-b Fitting data for EIS measurements under illumination with EEC Fig S11b.